AAS 19-582

ANALYSIS OF A SWARM DEPLOYMENT FOR VERY LOW EARTH ORBIT OPERATIONS

Bogdan Udrea*

A swarm of 12 space vehicles performs an Earth observation mission from a very low Earth circular orbit, at 200 km altitude. Deployment of the swarm from the upper stage of the launch vehicle has been identified as a critical phase of the mission. A deployment strategy has been found that sets up the swarm for success and results of the simulation performed with the Orbital Extrapolation Kit (Orekit) are presented to support this conclusion.

INTRODUCTION

A low cardinality swarm of 12 small satellites (smallsats) performs its mission in a very low Earth Orbit (vLEO) circular orbit of 200 km altitude. Dynamics of early orbit operations, including release from the launcher and the free motion immediately after deployment from the launcher, are analyzed with the purpose of "setting up the swarm for success." The major goal during early orbit is to mitigate risk while reducing and equalizing the expenditure of on-board resources such as propellant and communication subsystem power. Top level requirements will be derived for early operations for both the swarm members and the launch vehicle (LV) and its operation.

Q1. What is a "good" swarm member release strategy, within the constraints of a realistic launch scenario, that eliminates the risk of collision between swarm members and reduces the dispersion of the swarm during free motion?

Q2. What is the short term, up to 24 hours, evolution of the relative state vectors/relative orbital elements (ROEs) between swarm members, within the constraints of the mission?

Q3. What is a "good" schedule for the swarm members to deploy their stowed appendages while keeping the collision risk and swarm dispersion low?

Q4. Are there any existing or near-future sensors and algorithms, either space or ground based, that can aid in "setting up the swarm for success?"

The free motion interval specified in Q2 assumes that after 24 hours from deployment from the launcher the swarm members unstow their appendages, such as solar arrays and antennas, and commence the checkout/commissioning phase of the mission.

The resulting changes in the external configuration cause significant changes of the drag force experienced by the space vehicle (SV). Answers to Q3 seek to determine the schedule of appendage deployment so that the swarm is passively safe despite the abrupt changes in drag force and its uncertainty during appendage unstowing.

* Research Engineer, VisSidus Technologies, Inc, 601 Innovation Way, Daytona Beach, FL 32114.

Due to inevitabilities of operations in vLEO, such as rapid orbit decay, initial orbit determination (IOD) with either on-board or ground based means is a critical part of the CONOPS of the mission. Answers to Q4 provide requirements for on-board IOD sensors that can be used during the first 24 hours after ejection together with ground asset scheduling to perform rapid IOD and upload it to the swarm at the earliest opportunity. The goal is to find LV and SV systems configurations to enable swarm autonomy and, consequently, reserve the ground assets and "PowerPoint-in-the-loop" for emergencies.

Preliminary mission design indicates that each of the smallsats of this mission has a mass of ~100 kg and in its stowed configuration the SV volume is ~1 m×1 m×1 m. For the purpose of this paper the term smallsat refers to this mass and volume.

BRIEF OVERVIEW OF SPACE VEHICLES SWARMS

Swarm robotics is the field of engineering that deals with the design, implementation, and operation of multitudes of robots which collectively perform complex functions that would otherwise be unachievable by an individual swarm member. The complex functionality of a robot swarm is a result of local interactions between swarm members and interactions between swarm members and the environment. A few salient properties of robot swarms are: *1)* homogeneity, i.e., perfect or close similarity in form and function of the swarm members; *2)* scalability, i.e., execution of swarm's function changes only slightly with its cardinality; *3)* robustness, in the sense of fault tolerance, which relies on local communications, local sensing, and forsaking centralized control and the assignment of predetermined roles; and *4)* flexibility which is realized by coordination between members so that the swarm can execute widely varying functions[1].

To the knowledge of this author, Das et al.[2] used the term *swarm* in the context of a space mission with practical applications for the first time in 1998. They were discussing TechSat-21 [3-6], an Air Force Research Laboratory (AFRL) space-based radar mission, which would have flown formations of eight synthetic aperture radar (SAR) microsatellites with relative distances between a few tens of meters to a few kilometers. Unfortunately, TechSat-21 was cancelled in 2003, two years into the project, due to cost overruns[7]. Another high-profile multiple SV project, DARPA's Future, Fast, Flexible, Fractionated Free-flying Spacecraft United by Information Exchange, or System F6, was cancelled in 2013, after five years and $200M in expenditures. System F6 did not fit the definition of a swarm because its purpose was to demonstrate the distribution of functions of a large SV to a set of heterogeneous and fractionated smaller SVs. However, some parts of the System F6 research performed before cancellation could be applied to SV swarms[*].

An attempt to design SV swarms using a top down systems engineering approach has been published by Engelen et al.[8]. They take the position that SV swarms "*are specifically instructed **not** to maintain a tight geometric formation. Instead, they rely on the statistical given that within a certain window of time, at least one element would have been in the desired position in space to allow the swarm to gather data."* This definition seems to contradict the fundamental property of swarm robotics that the swarm's functionality is much more complex than that of a single member. Pang et al.[9] take a more practical approach of designing a swarm of nanosatellites based on the constraints of on-board electric power generation and the resulting bandwidth limitations for a radar payload. The cardinality of their swarm is a function of the mission duty cycle and it ranges from three to 82. For research work on swarm coordination and control Morgan et al.[10] define a swarm as a "*collection of hundreds to thousands of spacecraft with masses on the order of 100 g*"

[*] http://spacenews.com/35375darpa-cancels-formation-flying-satellite-demo/ (accessed Sep 14, 2018)

destined for applications such as "*massively distributed sensing applications.*" Consequently, their research focuses on swarm keeping, i.e., maintenance of relative positions and velocities between swarm members by rejecting environmental disturbances and collision avoidance. More recent research work on SV swarm coordination and control strategies[11] appears to be rehashing concepts already explored 15 years ago[12]. Only during the past few years several research groups, such as D'Amico's at Stanford University, have approached the analysis and design of SV swarms[13-19] within a systematic, mission-driven context.

In this author's opinion research and development of spacecraft swarms has been encountering two major adversities: *1) Causality dilemma*: the cost of development, launch, and on-orbit qualification of a single swarm member is prohibitive; a single member's extremely limited functionality has only a minor contribution to increasing the technology readiness level (TRL) of the swarm. On the other hand, the deployment of a swarm of spacecraft with low TRLs is perceived as highly risky because the performance of individual members and their means of interaction in orbit are unproven and *2) Dissonant relationship:* The goal of coordinated task planning, operation, and execution seems to be at odds with the current practice of space systems engineering. In a typical, single SV, mission resources are allocated relatively early in the project lifetime and are carefully tracked as the project advances. As such, it is challenging to cast, for example, propellant and error pointing budgets of a swarm within the context of institutional best practices and design guidelines[20].

The work presented here has been developed independently of the outstanding and thorough analysis and design work on swarm deployment recently published by Koenig and D'Amico[14, 18]. Similarities and differences are discussed below.

PROBLEM SET UP

The swarm studied here is composed of 12 SVs that operate in a circular orbit of 200 km altitude and carry Earth observation payloads. During nominal operations the swarm members operate within a few hundred meters from each other in a string-of-pearls configuration.

A generic LV upper stage, called a rocket body (RB), is sketched in Figure 1 together with most of the reference frames used in this paper. The reference frames are grouped in three categories, according to the location of their origin: central body-based frames, orbit-based frames, and SV body-based frames. The central body-based frames have the origin at the center of mass of the central body; viz., the Earth centered inertial (ECI) frame and the Earth-centered Earth fixed (ECEF) frame have the origin at the center of mass of Earth and are the typical ones used in astrodynamics. The only type of orbit-based frame employed in this study is the radial-transverse-normal (RTN) that has the origin at the center of mass (CoM) of a space object. Its radial (R) axis points along the position vector of the object, the normal (N) axis points along the angular momentum vector of the orbit, and the transverse (T) axis completes the right-hand system[21]. The origin of the RB body-fixed frame is at the CoM of the RB and its X axis is oriented along the longitudinal axis of the RB. Directions of the RB reference frames axes are specified by the respective RB's user guide. Payload deployers and the sensors mounted on the RB have orientations typically defined by their manufacturer/integrator. For example, CubeSat deployers such as the P-POD[22] or the CSD[23] follow the convention that their Z axis is the ejection axis, oriented radially out. On the other hand, the Mk II motorized LightBand[24] ejects the payloads along its X axis, also radially out.

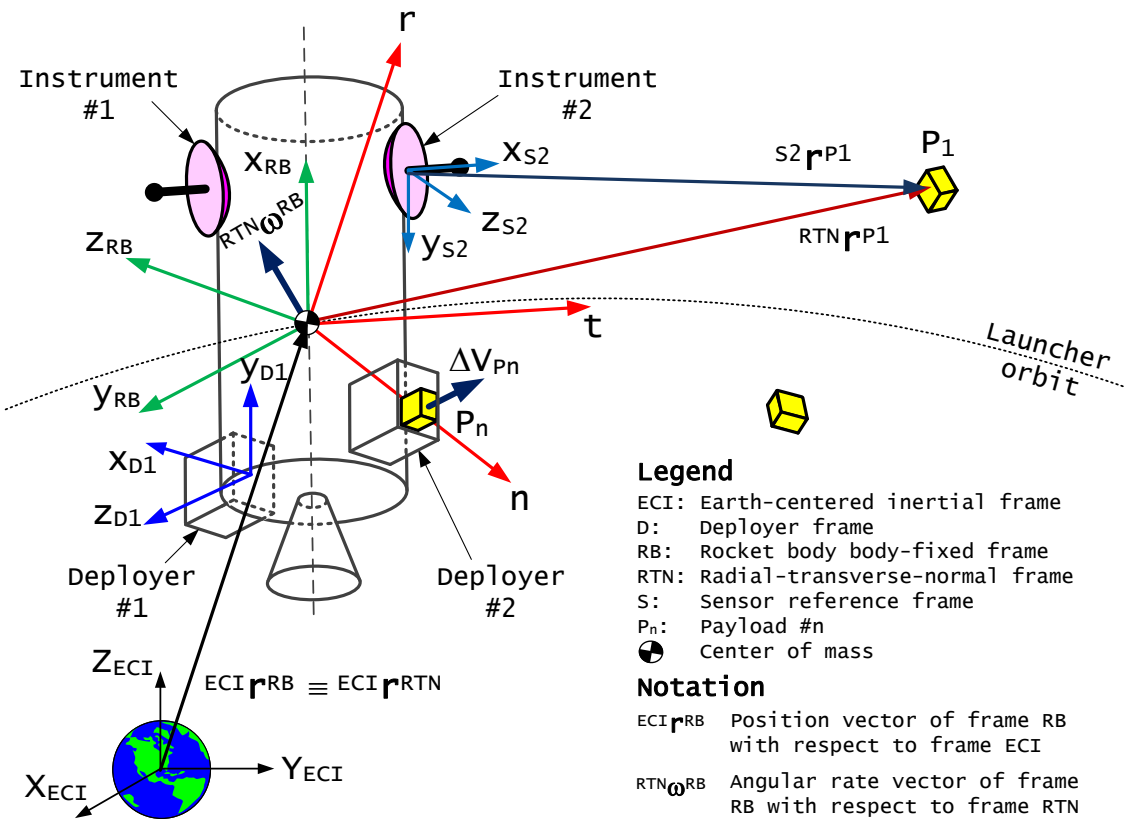

Figure 1. Sketch of the launcher upper stage, RB, with reference frames. For the work presented here the payloads are the space vehicles of the swarm.

Analysis of present and near future US-based commercial LVs has led to the selection of the SpaceX Falcon 9 due to its cost, performance,[25] and the potential of sharing the launch. Two SV-RB integration configurations have been considered and they are presented in Figure 2. Configuration (a) tightly integrates all 12 SVs in a single layer but leaves only a very small clearance between the SVs and between the SVs and the dynamic envelope of the payload fairing. Configuration (b) integrates four (4) SVs per launch adapter in three layers with ample clearance between SVs. Configuration (a) has been discarded because of the extremely small clearance between the stowed SVs and the difficulty of designing an adapter to share the launch. Consequently, configuration (b) has been carried forward with the ESPA[26-30] Grande secondary payload adapter together with the 24" Mk II motorized LightBand SV separation system [24]. Selection of configuration (b) imposes the operational constraint that deployment of the SVs is performed using the spin-stabilized attitude mode of the Falcon 9 second stage which supports a maximum angular rate of 30°/s. [25]

Conditions for bounded relative motion between a deputy (d) and a chief (c) SV have been presented by Koenig and D'Amico[15, 31] in terms of ROEs: $\delta a = 0$, and $\delta i_x = 0$, where $\delta a = (a_d - a_c)/a_c$ is the relative semimajor axis and $\delta i_x = i_d - i_c$ is the X component of the relative inclination vector.

It is assumed that after the first 24 hours from separation from the LV *1)* the SVs deploy their appendages, that include solar arrays and GPS antennas, and that each of them has the capability to independently determine its orbital state vector; *2)* each SV in the swarm starts a short but in-

tense commissioning period during which it can perform some orbital maneuvers, uncoordinated with the other members of the swarm; and *3)* after the commissioning phase they perform coordinated maneuver so that they assemble into a "loose formation."

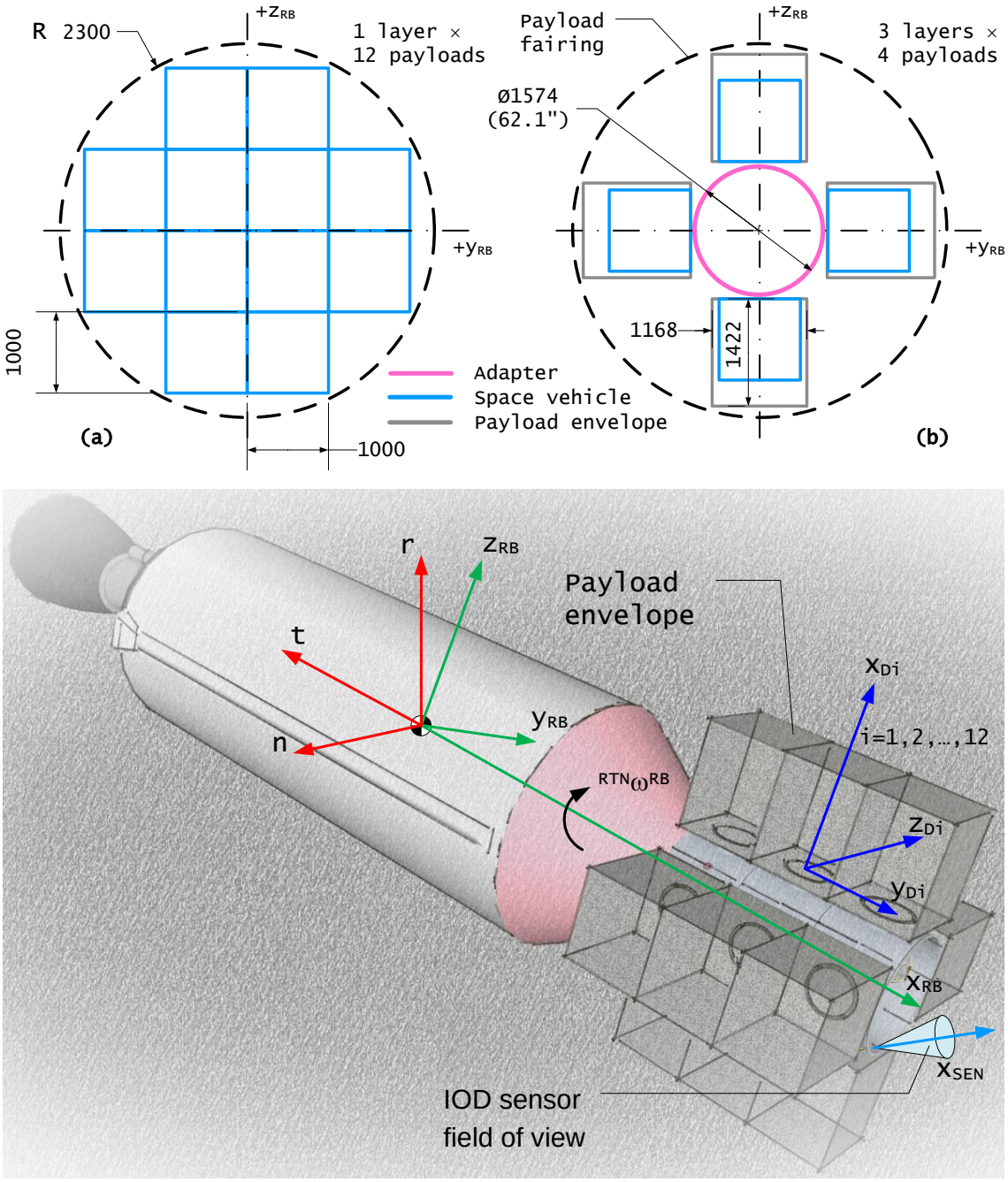

Figure 2. Top: SV – RB integration configurations. Bottom: configuration (b) on a SpaceX Falcon 9 second stage with ESPA Grande, 24" MkII motorized Lightband, and payload bounding boxes. Falcon 9 model by Giovane O is available on the Sketchup 3D Warehouse. *Dimensions in mm.*

Only the first 24 hours after separation from the RB are of interest here because during this period the SVs lack knowledge of their own orbital state vector and of their neighbors. Scenarios

that account for faults, such as one or more SVs fail to deploy their appendages or are incapable to determine their orbital elements are planned.

Simulations have been performed with an in-house developed Java code that uses libraries of version 9.2 of the Orbit Extrapolation Kit* (Orekit) and underlying numerical methods libraries of Hipparchus† version 1.3. A variable step, Dormand-Prince 8 (5,3) integrator is used with a minimum time step of 0.001 s and a maximum time step of 120 s.

A slightly elliptic injection orbit of 350 km by 250 km has been selected as a good compromise between decay due to drag during maximum solar activity and LV capabilities. The 96.33° inclination of the injection orbit is equal to that of the nominal, 200 km circular, Sun-synchronous orbit. The epoch of the first SV separation is at noon April 1, 2025.

Orbital perturbations due to a non-spherical gravitational potential with a J_2 term and drag have been considered. The Harris-Priester atmospheric model is employed with densities given by an NRL-MSISE model at solar maximum, anticipated in 2025, and with a day-night inflation factor of 30. The drag coefficient of the SV in its stowed configuration is $C_d = 2.1$ and its cross-sectional area is 1.0 m^2.

Space Vehicle Deployment Strategy

The energy stored in the springs of the separation mechanism is used to push the SV away from the RB during deployment. SVs deployed in the ±N (cross-track) directions of the RB orbit are slow to separate from the RB because the energy of the separation mechanism is applied to realize only a very small relative inclination change. Consequently, the relative motion is driven by the differential drag between the SV and the RB. Deployment in either the transverse (T) or radial (R) directions is more beneficial because the energy of the separation mechanism is applied to effect a reasonable change in relative orbital elements.

A few deployment simulations show that, within the assumptions made, the "best" separation direction is along the +R direction of the RTN frame because it results in a robust separation between the SVs and RB and a rapid deployment of all 12 SVs in the swarm. In this deployment scenario the X axis of the RB is antiparallel with the T axis of RTN, the RB rotates about its X axis, and each SV is separated at the instant its deployer X axis is parallel with the R axis of RTN. See Figure 2, bottom, for an illustration of the concept. Since SVs are integrated 90° from each other the fastest separation along the same RTN direction requires a cadence of 3 s at an RB angular rate of 30°/s (5RPM) which is the highest allowed for Falcon 9.

The SV separation speed is calculated with an expression[24] derived from the conservation of energy and momentum

$$v_{\text{sep}} = \sqrt{\frac{2\eta_s nE(m+M)}{mM}}, \tag{1}$$

where v_{sep} is the separation speed of the SV with respect to the RB, η_s is the separation efficiency, i.e., the efficiency of converting the spring-stored potential energy to kinetic energy, n is the number of springs, E is the energy stored in each spring, m is the SV mass, and M is the RB mass together with the mass of all the SVs still attached to it. To ensure a safe separation speed be-

* http://orekit.org/ (accessed Sep 14, 2018)
† https://www.hipparchus.org/ (accessed Sep 14, 2018)

tween SVs and the RB a number of 14, from a maximum of 24, separation springs have been used.[24] With the values of the simulation parameters shown in Table 1 the resulting deployment speeds vary between 0.512 m/s for the first SV and 0.513 m/s for the 12th. The change in deployment speed is due to the change in *M* after each SV deployment. In the simulations described here the separation speed have been be applied impulsively to each SV at the instant of separation together with the speed resulting from the rotation of the RB with respect to the RTN frame.

DEPLOYMENT ANALYSIS

A rather unsophisticated, zeroth order, analysis indicates that separation from RB at a cadence of 3 s at the orbital speed of the RB of ~7.74 km/s results in a separation distance between SVs of ~23.2 km. This analysis is confirmed by the plots of the relative orbits of SVs#2 to #12 with respect to SV#1 in the ECI frame together with the along-track separation between the same SV pairs, shown in Figure 3. The radii of the relative near-circular orbits, Figure 3-left, and the relative along-track distances, Figure 3-right, with respect to SV#1 are multiples of 23.2 km. It can be noticed that the amplitude of oscillations in the along-track distances (Figure 3-right) increases with the distance from SV#1 which can be explained by the slightly elliptic deployment orbit and the change in magnitude of the differential drag. Moreover, the distances between SVs increase slightly with time thus ensuring passive safety of the swarm. With the assumptions presented in the previous section, it seems that the swarm is "well behaved" during the first 24 hours after deployment. To verify this assertion the relative semimajor axis, δa, and the components of the relative inclination vector, δi_x and δi_y, have been analyzed. It can be noticed, see Figure 4, that these three ROEs are small, and they only slightly change during the first 24 hours after deployment. The finite value of the magnitude of the relative inclination vector is due to the rotational motion of the RB at SV separation which imparts a small "ΔV" in the N, cross-track, direction.

Table 1. Deployment Parameters

Parameter	Value	Unit	Comments
Perigee altitude	350.000	km	Trade between orbit decay and LV performance
Apogee altitude	250.000	km	Same as a above
Inclination	96.300	deg	Inclination of Sun-synch. nominal circ. orb. (200 km)
Arg. of periapsis	0.000	deg	
RAAN	0.000	deg	
Epoch day	April/01/2025	-	Possible solar max activity
Epoch time	12:00:00.000	-	
Mean anomaly	0.000	deg	
RB mass	4272.000	kg	Empty + 100 kg propellant
RB drag area	10.521	m^2	Cross-sectional area
RB drag coeff.	2.200	-	
RB Euler angles	(-90, 0, 0)	deg	3-2-1 seq. w/respect to RTN
RB angular rate	(-30, 0, 0)	deg/s	w/respect to RTN
SV mass	100.0	kg	Best current estimate
SV drag area	1.000	m^2	Stowed cube of 1 m side
SV drag coeff.	2.100	-	
Separation "ΔV"	0.512	m/s	n=14, $\eta_s = 0.9$, and E=1.02J.

Additional insight into the relative motion between SVs can be gained by analyzing it in the RTN frame. Positions in RTN frame are plotted vs. time for the SV#2-SV#1 and SV#12-SV#1 pairs together with the relative orbits in Figure 5. Only the first six hours, approx. four orbits, after deployment are shown for the purpose of clarity. The position in the transverse (T) direction oscillates about 23.2 km for SV#2 and about 255 km for the SV#12 motion with respect to SV#1. The amplitude of oscillations is a few hundred meters for SV#2 and a few

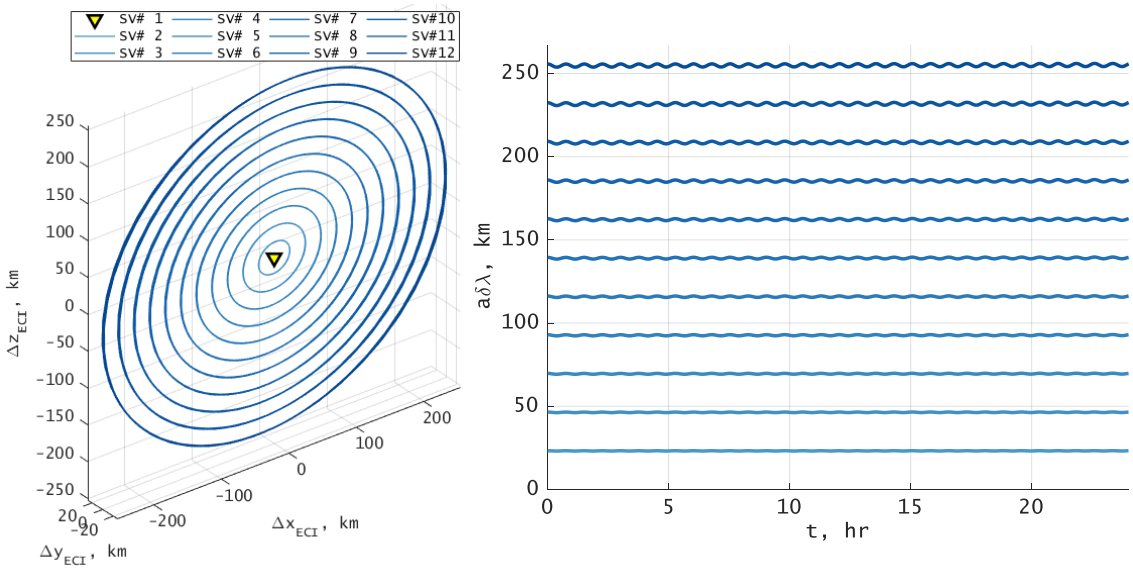

Figure 3. Relative orbits between SVs#2 - #12 and SV#1 (left) and along-track separation between the same pairs (right).

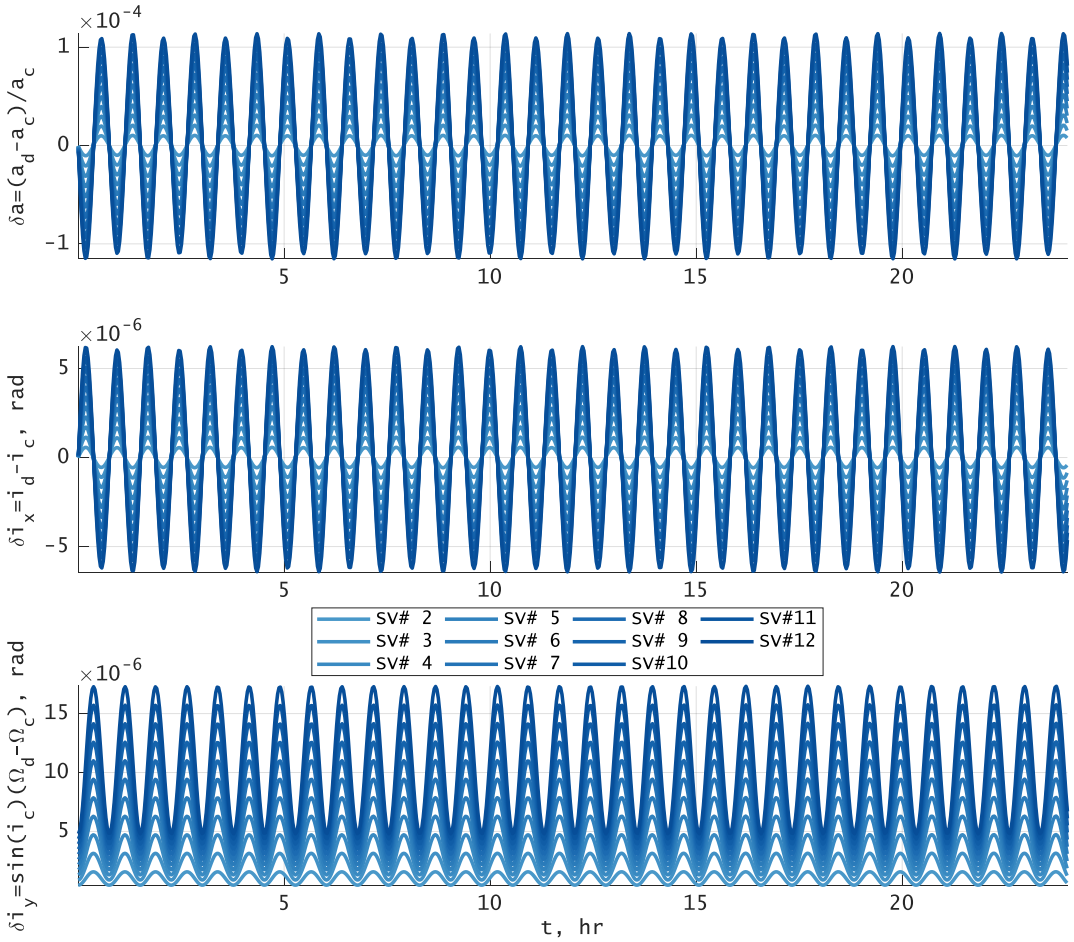

Figure 4. Relative semimajor axis and components of the inclination vector between SVs#2 - #12 and SV#1 during the first 24 hours after separation from the RB.

kilometers for SV#12. These results confirm the evolution of the along-track separation shown in Figure 3-right. Motion in the radial (R) and normal (N) directions also exhibit an oscillatory behavior with amplitudes that are proportional to the distance from SV#1. The relative orbits of all SV pairs, out of which only two are shown in Figure 5, are scaled version of each other.

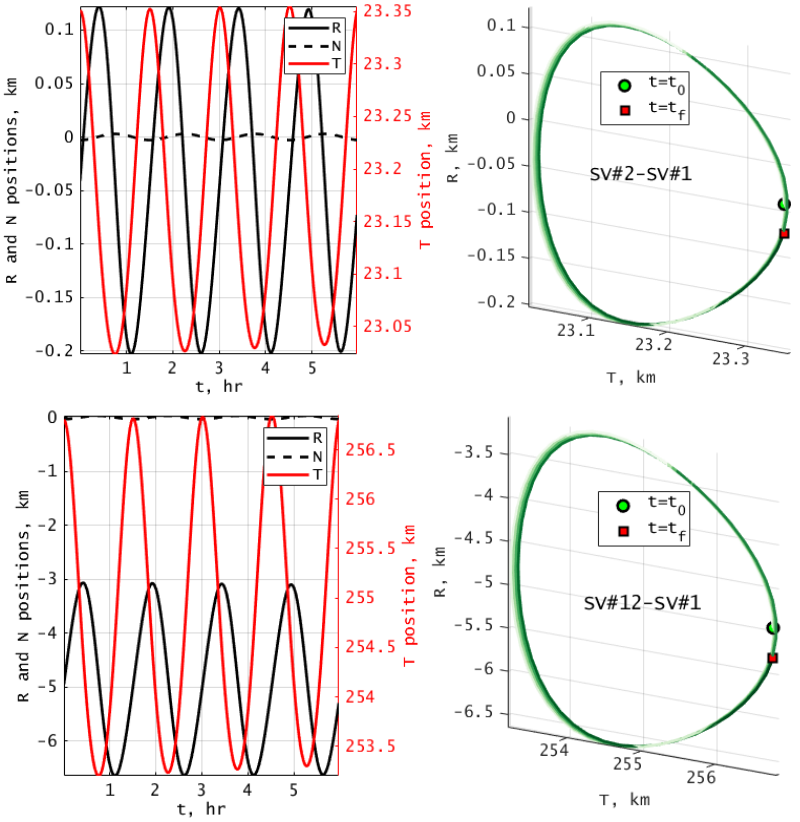

Figure 5. Relative RTN positions orbits between SVs#2 and SV#1 (top) and SV#12 and SV#1 (bottom). In the relative orbit plots the darker the shade the most recent the data.

Analysis of the deployment scenario has been concluded with the study of the relative motion in ROE space, as shown in Figure 6. For ease of interpretation the relative semimajor axis is plotted against, a somewhat unorthodox, difference between the along-track distance ($a\delta\lambda$) and the straight-line distance (d) between the SVs, as seen in Figure 6-top-left. The fish-like deformed epitrochoid pattern is almost symmetrical at the deployment of SV#2 and it deforms slightly with time: the "tail" of the fish twists along the intersection point under the influence of drag and Earth oblateness effects. Amplitudes of the radial motion ($a\delta a$) and along-track ($a\delta\lambda$) separation are roughly equal to the amplitudes of the SV#2-SV#1 radial (R) and transverse (T) components shown in in Figure 5. The normal-to-plane motion, Figure 6-top-right, has an expected and nearly circular pattern which remains almost unchanged during the first 24 hours after deployment. The radius of the circle is on the same order of magnitude with the amplitude of the position in the normal (N) direction of the RTN frame, shown in Figure 5. Last but not least, the in-plane motion, Figure 6-bottom, also exhibits an interesting, symmetric pattern that seems to be made of three lopsided lemniscates that intersect at a point. The lemniscates slightly expand and twist in time. It is interesting to note that similar patterns, specifically Bernoulli's lemniscates, were discovered by Willis and D'Amico[16], albeit in the RTN frame, in their study of low-thrust forced spiral relative trajectories in GEO.

In conclusion, the deployment strategy presented here answers questions Q1 and Q2 about setting up the swarm for success, see Introduction. During the first 24 hours after deployment: *1)* the along-track separation between consecutive swarm members is ~23.2 km that oscillate with a maximum amplitude of a few km; *2)* the distance between SVs grows by a few tens of meters, SV#2-SV#1, to a few hundred meters, SV#12-SV#1 during the first 24 hours; *3)* the amplitude of the cross-track motion is limited to a few tens of meters, SV#2-SV#1, to a few hundred meters, SV#12-SV#1; and *4)* the evolution of orbital elements is well understood and consistent with the

intuition and experience derived from relative motion and proximity operations. Question Q3, on the deployment sequence of the appendages the SVs and the consequences resulting from the change of aerodynamic drag area, will be answered in the later stages of the project, as the external configuration of the SVs converges. One certainty is that the SV with unstowed appendages are aerodynamically stable and have a lower drag area than in the stowed configuration. The answer to question Q4, about a sensor to aid in the rapid initial orbit determination (IOD) for the swarm members is answered in the next section.

Initial Orbit Determination Sensor

One of the general desiderata of spacecraft swarm missions is to operate with a high level of autonomy from ground control. Additionally, the mission described here operates in vLEO; i.e., at an altitude where irrecoverable orbit decay can take from a few days to a few weeks, depending on solar activity. Consequently, each swarm member benefits from good knowledge of its deployment orbit and of its neighbors before its global positioning system (GPS) is brought online.

If IOD can be performed immediately after deployment for each SV and the orbital elements broadcast to all the SVs then the swarm members could use an on-board orbit propagator to determine their own orbit and those of the other members.

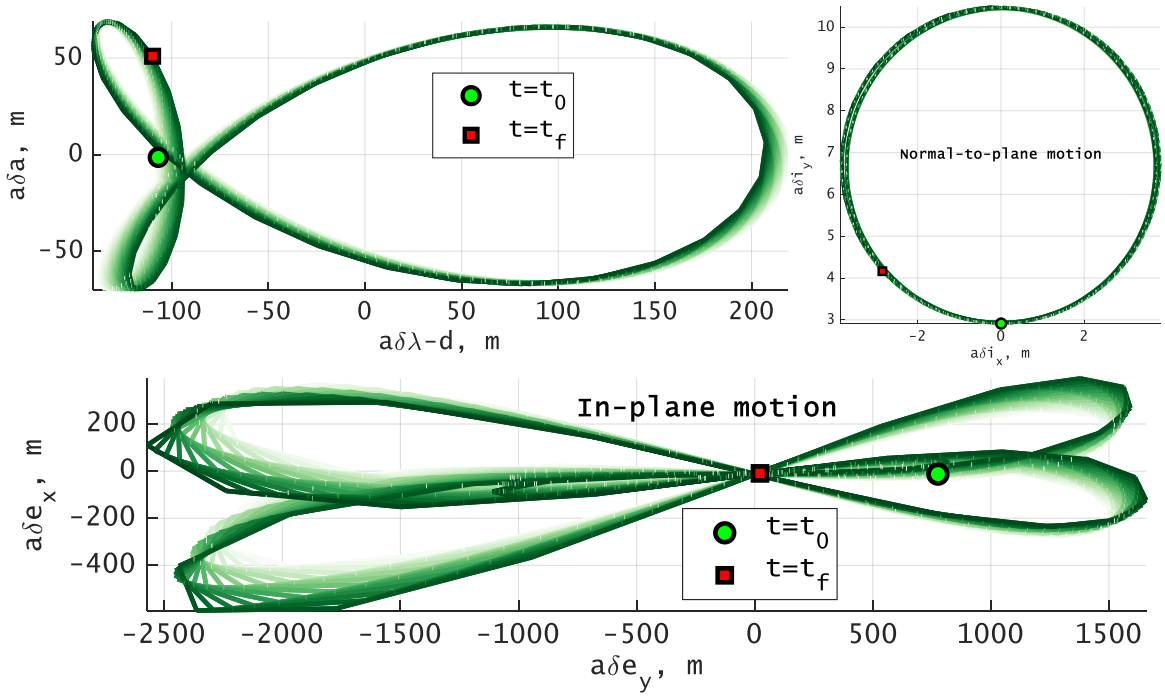

Figure 6. Relative motion in the ROE space between deputy SV#2 and chief SV#1 during 24 hours after deployment. The darker the shade the most recent the data.

An active sensor, either lidar or radar, can operate (almost) free of constraints such as target object illumination by the Sun and the presence of bright objects in the field of view (FoV). A trade study of commercial off-the-shelf (COTS) active sensors has been performed, that included criteria such as size, mass, power, potential for space qualification, and the availability of ASIC IP for customization. LeddarTech's Leddar M16-LED flash lidar has been selected for analysis; specifically the M16D-75B0010 with a FoV of 36°×6°, a maximum range of 62 m and the capability to provide highly accurate range maps to objects in the 16 segments of its FoV[32]. It has been as-

sumed that the IOD sensor is installed on the "uppermost" ESPA Grande ring and its boresight points towards the RB +X axis with a tilt of -56° about the RB Y axis (see Figure 2.)

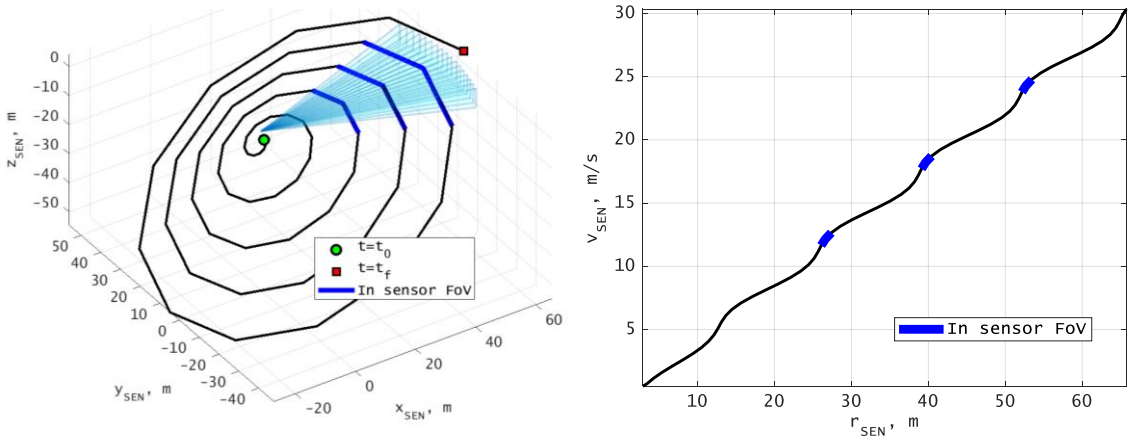

Figure 7. Motion of SV#1 (left) and speed vs. distance (right) in the reference frame of the IOD sensor. Sensor FoV is shown to maximum range in light blue and the visible segments of SV trajectory are highlighted in blue. Duration of the simulation is 60 s and the output time step is 1 s.

Results of the simulation of the motion of SV#1 with respect to the IOD sensor reference frame are shown in Figure 7. The expanding conical spiral motion is due to the coupling between the relative motion of the SV with respect to the RB and the rotational motion of the RB, of 30°/s, on which the sensor is rigidly mounted. Motion of the other 11 SVs with respect to the sensor frame follow the exact same pattern, the only difference being the position of the tip of the conical spiral.

Segments of the SV trajectory that lie within the FoV of the IOD sensor are highlighted in Figure 7. It can be noticed that in this, non-optimized, configuration the SV is visible only three times, for approx. 0.75 s, 1.25 s, and 1.5 s. The sensor has a sample rate of up to 100 Hz, which can be selected by the user and preliminary analysis shows that measurements above 10 Hz during these visibility passes are sufficient for relative state estimation. Estimation of the Cartesian relative state vector of the SV with respect to the RB with an unscented Kalman filter[*], on a similar scenario, has shown promising results.

Although somewhat speculative for the time being, one-way broadcast from the IOD sensor to the SVs is envisioned with the purpose of making available orbital state vectors of all the SVs that have been deployed. The implementation relies on modulating the light emitted by the sensor's active elements (LEDs) which is received by a set of photodiodes installed on the exterior of the SVs to provide full sky coverage.

UNCERTAINTY PROPAGATION

So far only nominal deployment conditions have been considered. This section discusses results of simulations that take into account uncertainties in the RB orbit and presents the next steps in accounting for other uncertainties such as those in the pointing of the RB, separation speed, and drag parameters. An uncertainty budget is presented in Table 2.

[*] Francisco Franquiz, private conversation.

Orekit provides field propagation (Java) methods that can be employed to perform dynamical propagation of initial and parametric uncertainties. As such, the practicing astrodynamicist, can significantly reduce the drudgery and time sink required to setup, run, and interpret Monte Carlo (MC) simulations. More importantly, the uncertainties can be fully tracked along the state trajectory of interest at any instant in time instead of at the end state as is the case in MC simulations.

The default field propagation method of Orekit employs automatic differentiation based on Taylor differential algebra[33-37] to propagate a set of uncertain initial conditions (ICs) and it has been used for the work presented here. Specifically, the effect of uncertainties in apogee and perigee altitudes, hence semimajor axis and eccentricity, inclination and right ascension of the ascending node (RAAN) on the orbital elements on individual SVs has been investigated. The values of uncertainties (3σ) are presented in Table 2 and highlighted (in peach puff.) Values highlighted in cornflower blue are the author's choice. They will be further refined as the project advances.

Table 2. Source and Size of Uncertainties

Src.	Parameter			Units	Ref. frame	Comments
	Name	Nominal	3σ			
RB orbit	Perigee alt.	200.00	10.00	km	ECI	From Falcon 9 Launch Vehicle Payload User's Guide.[25] Nominal inclination and RAAN are mission specific
	Apogee alt.	360.00	15.00	km		
	Inclination	96.30	0.10	deg		
	RAAN	0.00	0.10	deg		
Depl. speed	Efficiency	0.90	0.03	-	DEP	According to MkII Motorized Lightband User Manual[24]
	Energy	1.02	0.10	J		
	RB mass	4272.00	10.00	kg		
RB pointing	q_0	mission	TBD	-	ECI	Quaternion scalar component is q_0. "… *attitude and rate accuracies are developed as a mission-specific standard service*"[25]
	q_1	mission	TBD	-		
	q_2	mission	TBD	-		
	q_3	mission	TBD	-		
	ω_1	mission	TBD	rad/s		
	ω_2	mission	TBD	rad/s		
	ω_3	mission	TBD	rad/s		
SV drag	SV mass	100.00	0.25	kg	Body	Mass, drag coeff., and area define the SV ballistic coefficient. Drag force is expressed in the SV body-fixed frame.
	Drag coeff.	2.10	TBD	-		
	Area	1.00	TBD	m^2		
	Atm. dens.	model	TBD	kg/m^3		

The configuration of the orbit propagator is the same with those described in the previous section, the sample size is 1000 points, and the order of the Taylor series expansion is three. The order of expansion has been selected by starting at six and lowering it until results started changing significantly. Results of the uncertainty propagation for SV#1 are presented in Figure 8 and the results for the other 11 SVs are essentially the same. Within the assumptions presented here the effect of RB orbit uncertainties on a swarm member are bounded for the first 24 hours and are not a reason of concern. The "triple hump" of the perigee and apogee altitudes seen in Figure 8 is due to the day-night density variations at maximum solar activity.

Work in progress consists of including IC uncertainties of deployment speed magnitude, due to the deployment mechanism and SV and RB masses, see Eq. (1), and deployment speed orientation, due to RB pointing. The first step has been the analysis of the uncertainties in the deployment speed. In general, the uncertainty of a scalar valued func-

tion $f(x_1, x_2, \ldots, x_n)$, $x_i \in \mathbb{R}$, $i = 1, 2, \ldots, n$ with random and uncorrelated uncertainties σ_{x_i} $i = 1, 2, \ldots, n$ in its parameters is

$$\sigma_f = \sqrt{\sum_{i=1}^{n} \left(\frac{\partial f}{\partial x_i} \sigma_{x_i} \right)^2}, \tag{2}$$

where the partials of f with respect to its parameters are called the influence coefficients*. The influence coefficients of the deployment speed uncertainty are

$$\begin{aligned} \frac{\partial v}{\partial \eta} &= \frac{1}{2} \frac{v_{\text{sep}}}{\eta}, \qquad \frac{\partial v}{\partial E} = \frac{1}{2} \frac{v_{\text{sep}}}{E}, \\ \frac{\partial v}{\partial m} &= -\frac{\eta n E}{m^2 v_{\text{sep}}}, \quad \frac{\partial v}{\partial M} = -\frac{\eta n E}{M^2 v_{\text{sep}}}. \end{aligned} \tag{3}$$

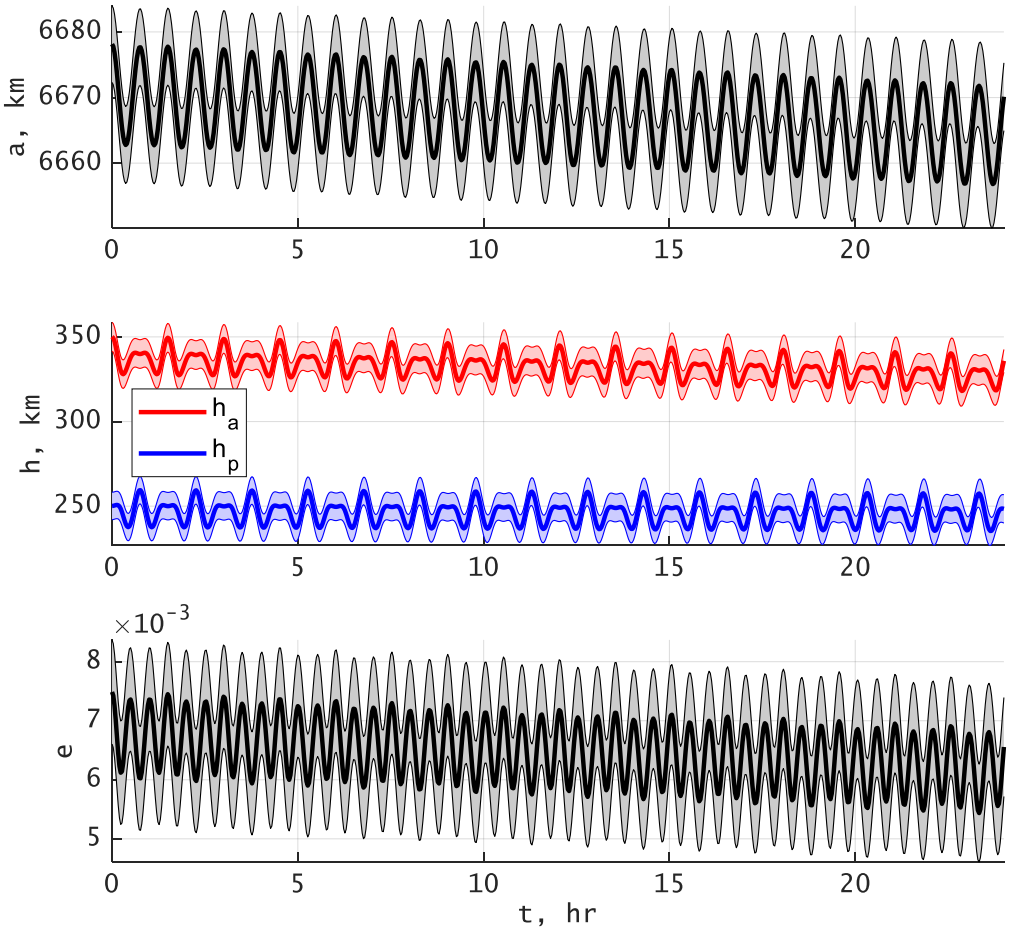

Figure 8. Uncertainties (1σ) bounds on the semimajor axis, perigee and apogee altitudes, and eccentricity of SV#1 during the first 24 hrs after deployment.

*https://www.itl.nist.gov/div898/handbook/ at the time of this writing, January 3, 2019, "due to a lapse in government funding, this and almost all NIST-affiliated websites will be unavailable until further notice"

With the values from Table 2 the standard deviation of the deployment speed varies between 0.0853 m/s for SV#1 and 0.0855 m/s for SV#12. The deployment speed magnitude uncertainty and the RB pointing uncertainty will be converted to uncertainties of orbital elements readily processed by the Orekit field propagation methods. At the same time, customization of Orekit force models is performed so that the effect of parametric uncertainties, such as the ballistic coefficient, used in the acceleration due to drag, and the mass, for the acceleration due to Earth's non-spherical gravitational potential, are also propagated.

As expertise with Orekit field propagation is gained it will be applied to the uncertainty analysis of the swarm dynamics in all phases of the mission.

CONCLUSIONS

Deployment strategies for a swarm of Earth observation SVs operating in a circular vLEO of 200 km altitude have been analyzed. Within the assumption made it has been found that the best strategy is deployment in the +R direction of the RTN frame. The relative motion is well understood and the distances between swarm members grow slowly, at rates between a few meters to a few tens of meters, during the first 24 hours after deployment. Propagation of uncertainties in the IC at RB orbit insertion have been propagated and they do not pose difficulties. Current work is performed on including additional IC uncertainties due to deployment mechanism and RB pointing at SV deployment and parametric uncertainties in the ballistic coefficient.

AKNOWLEDGEMENTS

The work presented here is supported by NASA STTR contract 80NSSC18P2136 and VisSidus Technologies IRAD resources. The encouragement and advice of our NASA STTR Technical Manager, Dr. Amir Rahmani (JPL) has been outstanding and it is much appreciated. We are also grateful for the support and words of wisdom we are receiving from Dr. Alan Lovell of AFRL.

Special acknowledgements go to the Orekit community, especially to Mr. Luc Maisonobe, the Orekit team leader at CS Communication & Systèmes. Luc provided the author prompt advice on both Orekit and modern Java programming practices. Merci beaucoup Luc!

REFERENCES

1. Sahin, E.; Spears, W. M.; Winfield, A. F. T., *Swarm Robotics: Second SAB 2006 International Workshop, Rome, Italy, September 30-October 1, 2006 Revised Selected Papers*. Springer: 2007.
2. Das, A.; Cobb, R.; Stallard, M., Techsat 21 - A revolutionary concept in distributed space based sensing. In *AIAA Defense and Civil Space Programs Conference and Exhibit*, AIAA: 1998.
3. Martin, M.; Stallard, M. In *Distributed satellite missions and technologies - The TechSat 21 program*, Space Technology Conference and Exposition, AIAA.
4. Burns, R.; McLaughlin, C. A.; Leitner, J.; Martin, M. In *TechSat 21: formation design, control, and simulation*, IEEE Aerospace Conference Proceedings, 2000.
5. Martin, M.; Klupar, P.; Kilberg, S.; Winter, J. In *Techsat 21 and Revolutionizing Space Missions Using Microsatellites*, SmallSat 2001, Logan, UT.
6. Winter, J. E.; Anderson, N. C. In *Distributed Aperture Implementation on the Techsat 21 satellites*, IEEE Aerospace Conference
7. Roth, J., Small Business Perspective (Microsat Systems). In *Government/Industry/Academic Relationships for Technology Development: A Workshop Report*, The National Academies Press: Washington, DC, 2005; p 95.
8. Engelen, S.; Gill, E. K. A.; Verhoeven, C. J. M. In *Systems engineering challenges for satellite swarms*, IEEE Aerospace Conference, Big Sky, MT, 5-12 March 2011; pp 1-8.

9. Pang, C. K.; Kumar, A.; Goh, C. H.; Le, C. V. In *Design and robust scheduling of nano-satellite swarm for synthetic aperture radar applications*, 13th International Conference on Control Automation Robotics and Vision (ICARCV), pp 705-710.
10. Morgan, D.; Chung, S.-J.; Blackmore, L.; Acikmese, B.; Bayard, D.; Hadaegh, F. Y., Swarm-Keeping Strategies for Spacecraft Under J2 and Atmospheric Drag Perturbations. *Journal of Guidance, Control, and Dynamics* **2012,** *35* (5), 1492-1506.
11. Sievers, M.; Madni, A. M. In *Agent-Based Flexible Design Contracts for Resilient Spacecraft Swarms*, 54th AIAA Aerospace Sciences Meeting, San Diego, CA, AIAA.
12. Schetter, T.; Campbell, M.; Surka, D., Multiple agent-based autonomy for satellite constellations. *Artif. Intell.* **2003,** *145* (1-2), 147-180.
13. Steindorf, L.; Scharnagl, J.; Kempf, F.; Schilling, K.; D'Amico, S. In *Constrained Low-Thrust Satellite Formation-Flying using Relative Orbit Elements*, 27th AAS/AIAA Space Flight Mechanics Meeting, San Antonio, TX.
14. Koenig, A.; D'Amico, S. In *Safe Spacecraft Swarm Deployment and Acquisition in Perturbed Near-Circular Orbits Subject to Operational Constraints*, 26th International Symposium on Space Flight Dynamics (ISSFD), Matsuyama, Japan.
15. Koenig, A.; D'Amico, S. In *Robust and Safe N-Spacecraft Swarming in Perturbed Near-Circular Orbits*, 26th International Symposium on Space Flight Dynamics (ISSFD), Matsuyama, Japan.
16. Willis, M.; D'Amico, S., Analytical approach to spacecraft formation-flying with low-thrust relative spiral trajectories. *Acta Astronautica* **2018,** *153*, 175-190.
17. Di Mauro, G.; Bevilacqua, R.; Spiller, D.; Sullivan, J.; D'Amico, S., Continuous maneuvers for spacecraft formation flying reconfiguration using relative orbit elements. *Acta Astronautica* **2018**.
18. Koenig, A. W.; D'Amico, S., Safe spacecraft swarm deployment and acquisition in perturbed near-circular orbits subject to operational constraints. *Acta Astronautica* **2018**.
19. Koenig, A. W.; Guffanti, T.; D'Amico, S., New State Transition Matrices for Spacecraft Relative Motion in Perturbed Orbits. *Journal of Guidance, Control, and Dynamics* **2017,** *40* (7), 1749-1768.
20. Ryschkewitsch, M. G., NASA Goddard Space Flight Center Mission Design Processes (The Green Book). 2005.
21. Vallado, D. A.; McClain, W. D., *Fundamentals of astrodynamics and applications*. 3rd ed.; Springer: New York, 2007; p xxi, 1055 p.
22. Pignatelli, D., Poly Picosatellite Orbital Deployer Mk. III Rev. E User Guide. 2014.
23. Whalen, M., Canisterized Satellite Dispenser Data Sheet. Corporation, P. S., Ed. 2013.
24. Whalen, M. *200785F MkII Motorized Lightband User Manual*; Planetary Systems Corporation: 2015.
25. SpaceX, Falcon 9 Launch Vehicle Payload User's Guide. 2 ed.; 2015.
26. DoD, Secondary Payload Planner's Guide for Use on the EELV Secondary Payload Adapter. Program, D. S. T., Ed. Department of Defense: 2001.
27. Maly, J. R.; Wilke, P. S.; Wegner, P. M.; Berenberg, L.; Sanford, G. E. In *ESPA from Concept to Flight Hardware*, SmallSat 2003, Logan, UT.
28. Caffrey, B., Using Rideshare to Launch CubeSats and ESPA Spacecraft. 2nd Planetary CubeSat Science Symposium: 2017.
29. Maly, J. R.; Sanford, G. E.; Williams, A.; Roybal, F. A.; Hultberg, R. In *ESPA Grande Qualification*, SmallSat 2018, Logan, UT.
30. Leon, C.; Anttonen, J., Evolved Expendable Launch Vehicle Rideshare User's Guide. (SMC/LE), S. a. M. S. C. L. S. E. D., Ed. El Segundo, CA, 2016.

31. Koenig, A. W.; D'Amico, S., Robust and Safe N-Spacecraft Swarming in Perturbed Near-Circular Orbits. *Journal of Guidance, Control, and Dynamics* **2018,** *41* (8), 1643-1662.
32. LeddarTech, Leddar M16. 2018.
33. Makino, K.; Berz, M., Remainder Differential Algebras and Their Applications. In *Computational Differentiation: Techniques, Applications, and Tools*, Berz, M.; Bischof, C.; Corliss, G.; Griewan, A., Eds. Society for Industrial and Applied Mathematics: 1996.
34. Berz, M. In *From Taylor series to Taylor models*, Beam stability and nonlinear dynamics, Santa Barbara, CA, pp 1-23.
35. Wittig, A.; Di Lizia, P.; Armellin, R.; Makino, K.; Bernelli-Zazzera, F.; Berz, M., Propagation of large uncertainty sets in orbital dynamics by automatic domain splitting. *Celestial Mechanics and Dynamical Astronomy* **2015,** *122* (3), 239-261.
36. Roberto, A.; Lizia, P. D.; Wittig, A.; Morselli, A.; Valli, M., Uncertainty Propagation Using Differential Algebra. In *Workshkop on Nonlinear Uncertainty Propagation using Differential Algebra*, 2015.
37. Bignon, E.; Mercier, P.; Azzopardi, V.; Pinede, R. In *Accurate numerical orbit propagation using Polynomial Algebra Computational Engine PACE*, 25th International Symposium on Space Flight Dynamics ISSFD, Muenchen, Deutschland.